ELSEVIER

Applied Surface Science 162–163 (2000) 42–47

applied surface science

www.elsevier.nl/locate/apsusc

Surface electronic transport on silicon: donor- and acceptor-type adsorbates on Si(111)-$\sqrt{3} \times \sqrt{3}$-Ag substrate

Shuji Hasegawa [a,b,*], Koji Tsuchie [a], Keinosuke Toriyma [a], Xiao Tong [a], Tadaaki Nagao [a,b]

[a] *Department of Physics, School of Science, University of Tokyo, 7-3-1 Hongo, Bunkyo-ku, Tokyo 113-0033, Japan*

[b] *Core Research for Evolutional Science and Technology, The Japan Science and Technology Corporation, Kawaguchi Center Building, Hon-cho 4-1-8, Kawaguchi, Saitama 332-0012, Japan*

Abstract

Adsorptions of monovalent atoms (noble and alkali metals) of submonolayer coverages (0.1–0.2 ML) on the Si(111)-$\sqrt{3} \times \sqrt{3}$-Ag surface commonly induced similar $\sqrt{21} \times \sqrt{21}$ superstructures, all of which exhibited high electrical conductances. Common processes seem to work among these adsorbates in such phenomena; the valence electrons of the adsorbates are transferred to the substrate surface-state bands (carrier doping). On the contrary, adsorption of C_{60} molecules on the $\sqrt{3} \times \sqrt{3}$-Ag surface reduced the conductance, presumably because conduction electrons in the surface-state band of the substrate are transferred to the molecules due to their strong electronegativity (acceptor-type adsorbates). © 2000 Elsevier Science B.V. All rights reserved.

PACS: 73.25.+i; 73.20.−r; 73.20.At

Keywords: Surface electrical transport; Silicon; Silver; Alkali metals; Fullerenes

Si(111)-$\sqrt{3} \times \sqrt{3}$-Ag surface is one of the most popular and long-standing targets in surface science. After a long controversy on its atomic arrangement, a model called Honeycomb-Chained Triangle (HCT) structure having $p31m$ symmetry was accepted to be consistent with all experimental and theoretical results hitherto reported [1]. But, very recently, it is turned out by theoretical calculations that it is not the end; the HCT is not the ground-state structure. So-called Inequivalent Triangle (IET) structure having $p3$ symmetry, in which a mirror symmetry in the HCT structure is broken, is found to be more energetically favorable [2]. This prediction is confirmed by low-temperature (62 K) scanning tunneling microscopy (STM) observations [2,3]. The IET structure is characterized by twisted Si trimers and different-sized Ag triangles. These ideas had already been proposed, but in incomplete manners, from electron diffraction analyses [4,5]. However, these had seemed to be shadowed by the $p31m$-symmetry HCT model. The present comprehensive picture of this surface is that the HCT structure is stable only around room temperature (RT) or higher temperatures, but a phase

* Corresponding author. Department of Physics, School of Science, University of Tokyo, 7-3-1 Hongo, Bunkyo-ku, Tokyo 113-0033, Japan. Tel.: +81-3-5841-4167.

E-mail address: shuji@surface.phys.s.u-tokyo.ac.jp (S. Hasegawa).

0169-4332/00/$ - see front matter © 2000 Elsevier Science B.V. All rights reserved.
PII: S0169-4332(00)00168-9

transition should proceed from the HCT to the IET structure at a lower temperature, nature of which transition is still unclear.

We can trace a long history also about its electronic structure. Early stages of direct- and inverse-photoemission spectroscopies confirmed its semiconducting nature [6,7], which was a strong basis for assertion of its Ag saturation coverage to be one monolayer (ML); even number of valence electrons in the $\sqrt{3}\times\sqrt{3}$ unit cell (three from Ag atoms and nine from dangling bonds of three Si atoms) completely fill surface-state bands. Theoretical calculations also showed an energy gap around the Fermi level (E_F) in the surface- state band structure [8–10]. But re-examinations of photoemission measurements under different conditions revealed its metallic character [11–13], that was, however, believed to come from an extrinsic reason [11,12]. Recent inverse photoemission and STS measurements also indicate its metallic character [14,15]. On the other hand, the recent first-principles calculations show a semi-metal band structure for the HCT model and an intrinsic metallic character for the IET model [2]. The bottom of an upward-dispersive surface-state band, called S_1 band, is located just at E_F for the HCT, while it is slightly below E_F, making a small electron pocket, for the IET model.

This characteristic surface-state band S_1, stemming mainly from Ag 5p orbitals [16], plays main roles in electronic phenomena on this surface; so-called electron standing waves at step edges and domain boundaries in STM images reveal its free electron-like nature in two dimensions [17]. Electrical conduction through this surface-state band is detectable even by a primitive four-point probe method; very small amount of Ag or Au atoms (less than 0.1 ML) adsorbed on this $\sqrt{3}\times\sqrt{3}$-Ag surface donate electrons into the S_1 band, resulting in an increase of conductance [13,18,19]. Further adsorption of excess Ag or Au (0.1–0.2 ML) induces a new order, $\sqrt{21}\times\sqrt{21}$ structures, which enhance the conductance further [19–22].

In this paper, we report conductance changes induced by adsorptions of noble metals (Au, Ag, Cu), alkali metals (K and Cs), and C_{60} molecules on the $\sqrt{3}\times\sqrt{3}$-Ag substrate, together with discussions on the photoemission and STS data to clarify the mechanism of the conductance changes.

Electrical conductances were measured in situ by a four-point probe method with around 10-mm-probe spacings in ultrahigh vacuum chambers [23–25], equipped with reflection-high-energy electron diffraction (RHEED) and evaporation sources. Silicon wafers used were typically $20\times5\times0.4$ mm^3 in size and 10–100 Ω cm in resistivity at RT of both of n- and p-types. There were no qualitative differences in the results presented here between n- and p-type wafers. All the measurements were done at RT except for Fig. 1(b). After making the clean 7×7 surface by flashing at 1200°C several times, the $\sqrt{3}\times\sqrt{3}$-Ag surface was prepared by depositing just 1 ML or more than 1 ML of Ag at 500°C. Precise coverage controls were done by in-situ RHEED observations during the Ag deposition with a constant rate. After the completion of the $\sqrt{3}\times\sqrt{3}$-Ag surface, the sample was cooled down to RT for 1 h, and then additional noble-metal atoms or C_{60} molecules were deposited in it.

Fig. 1 shows conductance changes of Si wafers having the $\sqrt{3}\times\sqrt{3}$-Ag surface measured as a function of deposited coverage of noble metals, (a) Au, (b) Ag, and (c) Cu, respectively. Surface structures intermittently observed by RHEED in the course of depositions are also indicated on the corresponding coverages. It should be noted that these three cases show some common behaviors; when the depositions start, the conductances begin to increase steeply, make maximums around 0.15 ML coverages, then, drop up to around 0.4 ML coverages, and finally turn to rise again beyond $\sim$0.5 ML coverages. Around the conductance peaks at 0.07–0.25 ML, the $\sqrt{21}\times\sqrt{21}$ superstructures commonly appear. After these structures disappear by further depositions, $\sqrt{3}\times\sqrt{3}$ superstructures appear, which are different from the initial $\sqrt{3}\times\sqrt{3}$-Ag structure in RHEED intensity ratios among the super-lattice spots. The final stages of gradual increase in conductance over $\sim$0.5 ML coverage correspond to degradations of the $\sqrt{3}\times\sqrt{3}$ structures. These results indicate that only the $\sqrt{21}\times\sqrt{21}$ phases are highly conductive.

We have already reported the electronic-state evolution during the formation of the $\sqrt{21}\times\sqrt{21}$ superstructure with Au deposition on the $\sqrt{3}\times\sqrt{3}$-Ag surface at RT, investigated by photoemission spectroscopies [13]. When the Au coverage is less than 0.1 ML where the $\sqrt{21}\times\sqrt{21}$-RHEED pattern does not

yet appear, the parabolic S_1 band of the $\sqrt{3}\times\sqrt{3}$-Ag substrate shifts down in energy position, meaning, larger number of electrons are trapped in this surface-state band. This is because the Au adsorbates donate electrons into the S_1 band, leading to an increase of conductance. (Similar carrier doping phenomena are observed also in the case of deposition of small amounts of Ag on the $\sqrt{3}\times\sqrt{3}$-Ag surface [18].) With further deposition of Au, the $\sqrt{21}\times\sqrt{21}$ structure begins to appear and complete around 0.2 ML coverage, and correspondingly, the S_1 band splits into two metallic dispersive bands, S_1' and S_1^* bands. The S_1^* band has a larger Fermi wavenumber, causing a further increase of conductance. Larger number of electrons in the S_1' and S_1^* bands also come from the Au adatoms. Thus, electron transfer from the adsorbates to the substrate plays essential roles in forming the $\sqrt{21}\times\sqrt{21}$ superstructure and conductance increase. Positively charged Au adatoms are arranged periodically to make the superstructure. The surface space-charge layer turns out to play no roles in the conductance increase.

Recently, these electronic evolutions are observed also in the case of Cu adsorption [21]. The energy shift of the S_1 band due to dilute Cu adsorbates, and the formation of the dispersive metallic bands S_1' and S_1^* are also confirmed with Cu deposition. Since the $\sqrt{21}\times\sqrt{21}$ superstructure for Cu adsorption is less stable than that for Au adsorption, only a part of surface is covered with the $\sqrt{21}\times\sqrt{21}$ phase for the Cu case, while the Au-induced $\sqrt{21}\times\sqrt{21}$ structure covers the whole surface. This is the reason for a smaller increase of conductance for Cu case (Fig. 1c) than for Au case (Fig. 1a). Photoemission measurements for the Ag-induced $\sqrt{21}\times\sqrt{21}$ phase at low temperatures are now in progress.

Fig. 2a and b show changes in conductance of a Si wafer during K and Cs adsorptions, respectively, onto the Si(111)-$\sqrt{3}\times\sqrt{3}$-Ag surface at RT, together with changes in RHEED patterns observed in the separate runs of deposition under the same condition

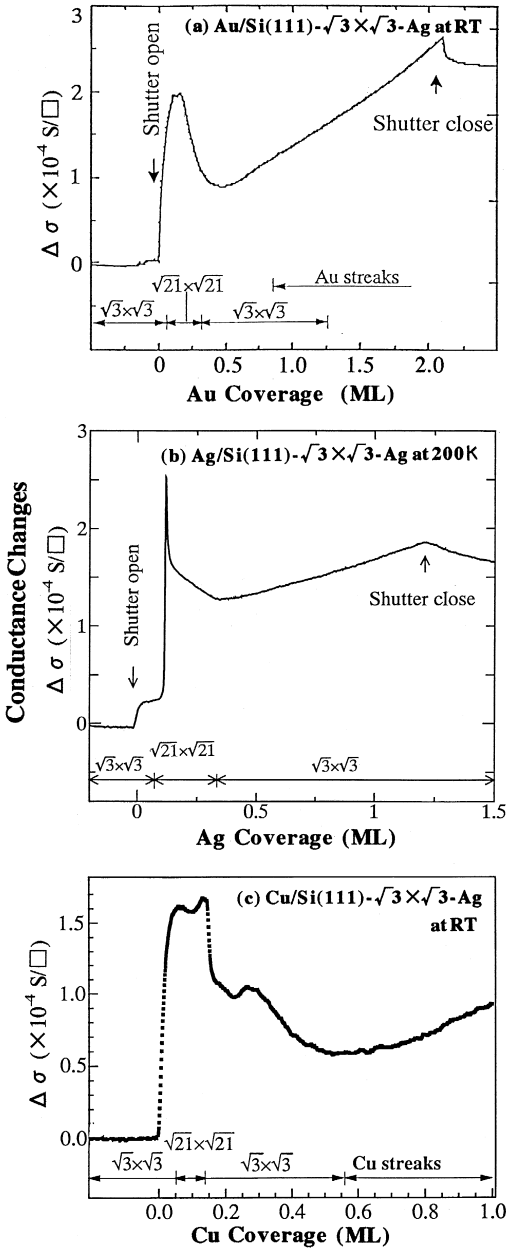

Fig. 1. Changes in sheet conductance of Si wafers during depositions of (a) Au, (b) Ag, and (c) Cu on the Si(111)-$\sqrt{3}\times\sqrt{3}$-Ag surface at (a),(c)RT and at (b) 200 K, respectively. By making a small DC current I (10–100 μA) flow through the Si wafer from the end clamps, a voltage drop V between a pair of Ta wires contacted to the central area of the wafer surface was measured to deduce the resistance $R = V/I$ [23–25]. Such measurements were done continuously during the metal depositions. Conductance change $\Delta\sigma$ was calculated from the resistance by $\Delta\sigma = (1/R - 1/R_0)(W/L)$, where R_0 is the initial resistance of the $\sqrt{3}\times\sqrt{3}$ surface before the noble-metal depositions, W and L are the width of the Si wafer and the spacing between the Ta-wire voltage probes, respectively.

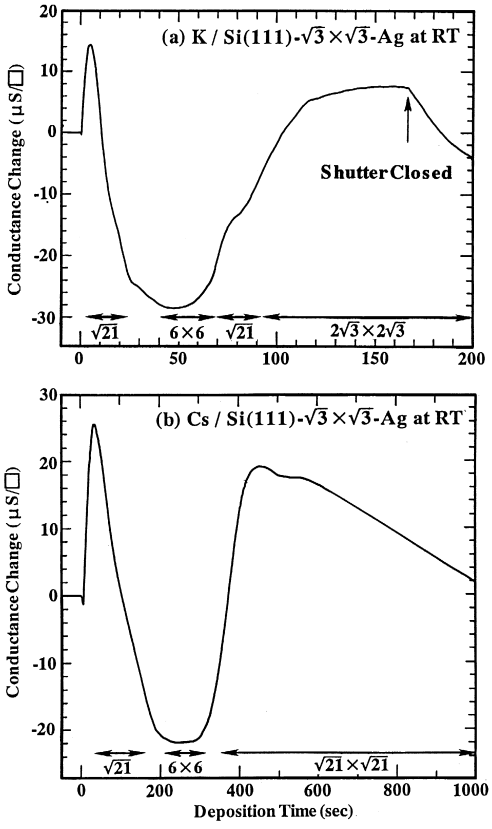

Fig. 2. Changes in sheet conductance of a Si wafer, measured in a similar way as in Fig. 1, during depositions of (a) K and (b) Cs on the Si(111)-$\sqrt{3}\times\sqrt{3}$-Ag surface at RT, respectively [26]. The $\sqrt{3}\times\sqrt{3}$-fractional-order spots in RHEED were always observed through the depositions.

[26]. The alkali metals were evaporated from commercially available dispensers (from SAES Getters). The results are shown just as a function of deposition time, because the coverages of alkali-metals were not precisely estimated. The conductances as well as the structures change in similar ways for both adsorptions; the conductance rises steeply at the beginning to reach a maximum, which corresponds to the appearance of a $\sqrt{21}\times\sqrt{21}$ superstructure. Then, the conductance decreases steeply to a minimum, less than the initial value, which corresponds to the disappearance of the $\sqrt{21}\times\sqrt{21}$ superstructure, changing into a $\sqrt{3}\times\sqrt{3}$ structure. Around the conductance minimum, a 6×6 superstructure appears. With further adsorptions, the conductance rises again, during which the 6×6 superstructure converts into a $\sqrt{21}\times\sqrt{21}$structure again. This RHEED pattern continues with further deposition of Cs, while it changes into a $2\sqrt{3}\times2\sqrt{3}$ superstructure for the K-adsorption case.

The changes in structure and conductance at the initial stages of deposition of K and Cs look quite similar to the cases of noble-metal adsorptions in Fig. 1, though the later stages of alkali-metal depositions show more complicated behaviors. Although the changes in surface electronic states during the alkali-metal adsorptions have not yet been investigated, the formation of similar $\sqrt{21}\times\sqrt{21}$structures as well as the steep conductance increase strongly suggest that the common mechanisms can be applied to these phenomena as in the case of noble-metal adsorptions, because of the common feature of monovalency of adsorbates. As confirmed by photoemission measurements in the cases of noble-metal-induced $\sqrt{21}\times\sqrt{21}$superstructures, metallic surface-state bands are presumably formed to make the surface highly conductive also in the case of K- and Cs-induced $\sqrt{21}\times\sqrt{21}$superstructures. These phenomena may be raised by a fact that the adatoms provide the valence electrons to the substrate to modulate the surface-state band of the initial $\sqrt{3}\times\sqrt{3}$-Ag structure.

In fact, none of Ca, Mg, and In adsorptions on the $\sqrt{3}\times\sqrt{3}$-Ag surface induce any new superstructures or conductance increases; the $\sqrt{3}\times\sqrt{3}$-Ag structure is gradually destroyed as the coverage of the divalent or trivalent atoms increases [27], and the conductance monotonically decreases from the beginning of the deposition to reach a smaller value of around 1 ML coverage of these metals. These comparative observations convince us of the importance of monovalency of the adatoms to induce the $\sqrt{21}\times\sqrt{21}$superstructures and also to raise the surface conductance.

We made similar measurements of conductance during deposition of C_{60} molecules on the $\sqrt{3}\times\sqrt{3}$-Ag substrate at RT. The results are shown in Fig. 3, where the coverage of C_{60} molecules is defined to be 1.1×10^{14} cm^{-2}, a number density for closed packing in C_{60} monolayer. The conductance begins to decrease steeply as the deposition starts, and make a minimum around 0.5 ML coverage, and then, turn to increase with further deposition. This behavior sharply contrasts to the monovalent-metal adsorptions in Figs. 1 and 2.

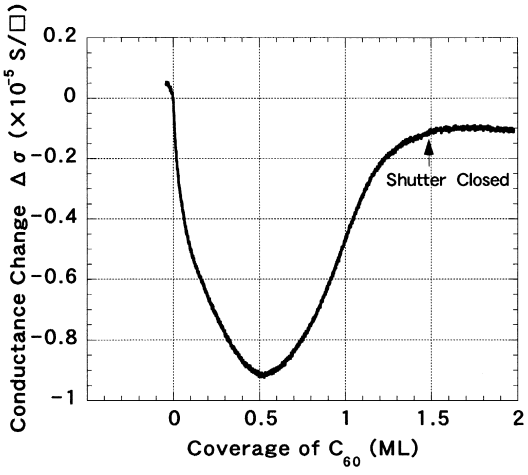

Fig. 3. Changes in sheet conductance of a Si wafer, measured in a similar way as in Fig. 1, during depositions of C_{60} molecules on the Si(111)-$\sqrt{3}\times\sqrt{3}$-Ag surface at RT. C_{60} molecules (more than 99.9% in purity) were sublimated at a rate of about 0.1 ML/min from a Knudsen cell held at 400°C [28]. Note that 1 ML of C_{60} was defined as the molecule density for which the available surface area was completely covered with a close-packed hard-sphere layer with the intermolecular spacing in bulk C_{60} crystals, 1.005 nm.

From STM observations of this adsorption process [28], the conductance changes in Fig. 3 are correlated to the adsorption structures. At the initial stage of less than 0.1 ML coverage where the conductance steeply decreases, the C_{60} molecules adsorb only at step edges on the $\sqrt{3}\times\sqrt{3}$-Ag, while no molecules are found on terraces. The molecules at step edges are so tightly bound to the substrate that free rotation of each C_{60} is forced to stop, which enables STM to observe internal structures of individual molecules. In a coverage range 0.1–0.5 ML, two-dimensional C_{60} islands grow on terraces where the molecules are arranged in $\sqrt{21}\times\sqrt{21}$ periodicity (and partly in $3\sqrt{3}\times 3\sqrt{3}$ periodicity). At a higher coverage range around 1 ML, the surface is wholly covered by C_{60} monolayer. Individual C_{60} adsorbed on terraces does not exhibit its internal structure in STM images at RT, meaning their fast free rotation at each position.

How can we understand the decrease in conductance by C_{60} adsorption observed in Fig. 3? It is known that C_{60} chemisorbs strongly on noble metal surfaces due to significant charge transfer (around one electron per molecule) to C_{60} from the metal surfaces, thereby forming C_{60} anions, so that its lowest unoccupied molecular orbitals (LUMO) is partially occupied by electrons, which is actually observed by photoemission spectroscopy [29]. This is due to strong electronegativity of C_{60}. Also on the clean Si(111) and Si(100) surfaces, C_{60} makes strong chemical bonds with substrate dangling bonds, but only fractional electronic charge is transferred from the substrate, so that partial filling of the LUMO is not observed by photoemission spectra [30]. On the Si(111)-$\sqrt{3}\times\sqrt{3}$-Ag surface, there are no dangling bonds, so that C_{60} is very weakly bound on terraces, which is shown by STM observations [28,31] and core-level spectroscopy [32]. However, it is not a physisorption. Since it is observed that the E_F approaches toward the LUMO peak in STS spectra [33] and some vibration energies are shifted in high-resolution electron-energy-loss spectra [34], it can be said that a very small amount of charge is transferred to C_{60} from the substrate. In other words, some conduction electrons in the surface-state band S_1 of the substrate are trapped by C_{60} adsorbates. This is presumably the reason for the conductance decrease observed in Fig. 3. This conductance decrease cannot be explained in terms of band bending induced by C_{60} adsorption, because the surface space-charge layer under the $\sqrt{3}\times\sqrt{3}$-Ag surface should be a stronger hole-accumulation layer due to excess negative charges of C_{60} adsorbates, which should lead to a conductance increase, opposite to the observed decrease. Therefore, it can be said that C_{60} acts as an acceptor to compensate conduction electrons in the surface-state band of the substrate.

Acknowledgements

Prof. M. Tsukada and Dr. H. Aizawa of the University of Tokyo, and Dr. T. Nakayama of RIKEN are acknowledged for their valuable discussions. This work has been supported in part by Grants-In-Aid from the Ministry of Education, Science, Culture, and Sports of Japan, especially through the Creative Basic Research (No. 09NP1201) conducted by Prof. K. Yagi of Tokyo Institute of Technology. We have been supported also by the Core Research for Evolu-

tional Science and Technology of the Japan Science and Technology conducted by Prof. M. Aono of the Osaka University and RIKEN.

References

[1] V.G. Lifshits, A.A. Saranin, A.V. Zotov, Surface Phases on Silicon, Wiley, Chichester, 1994.
[2] H. Aizawa, M. Tsukada, N. Sato, S. Hasegawa, Surf. Sci. 429 (1999) L509.
[3] N. Sato, T. Nagao, S. Hasegawa, Surf. Sci. 442 (1999) 65.
[4] A. Ichimiya, S. Kohmoto, T. Fujii, Y. Horio, Appl. Surf. Sci. 41/42 (1989) 82.
[5] H. Over, S.Y. Tong, J. Quinn, F. Jona, Surf. Rev. Lett. 2 (1995) 451.
[6] T. Yokotsuka, S. Kono, S. Suzuki, T. Sagawa, Surf. Sci. 127 (1983) 35.
[7] J.M. Nicholls, F. Salvan, B. Reihl, Phys. Rev. B 34 (1986) 2945.
[8] S. Watanabe, M. Aono, M. Tsukada, Phys. Rev.B 44 (1991) 8330.
[9] Y.G. Ding, C.T. Chang, K.M. Ho, Phys. Rev. Lett. 67 (1991) 1454.
[10] Y.G. Ding, C.T. Chang, K.M. Ho, Phys. Rev. Lett. 69 (1992) 2452.
[11] L.S.O. Johansson, E. Landemark, C.J. Karlsson, R.I.G. Uhrberg, Phys. Rev. Lett. 63 (1989) 2092.
[12] L.S.O. Johansson, E. Landemark, C.J. Karlsson, R.I.G. Uhrberg, Phys. Rev. Lett. 69 (1992) 2451.
[13] X. Tong, C.-S. Jiang, S. Hasegawa, Phys. Rev. B 57 (1998) 9015.
[14] J. Viernow, M. Henzler, W.L. O'Brien, F.K. Men, F.M. Leibsle, D.Y. Petrovykh, J.L. Lin, F.J. Himpsel, Phys. Rev. B 57 (1998) 2321.
[15] H.H. Weitering, J.M. Carpinelli, Surf. Sci. 384 (1997) 240.
[16] H. Aizawa, M. Tsukada, Phys. Rev. B 59 (1999) 10923.
[17] N. Sato, T. Nagao, S. Takeda, S. Hasegawa, Phys. Rev. B 59 (1999) 2035.
[18] Y. Nakajima, S. Takeda, T. Nagao, S. Hasegawa, X. Tong, Phys. Rev. B 56 (1997) 6782.
[19] X. Tong, S. Hasegawa, S. Ino, Phys. Rev. B 55 (1997) 1310.
[20] C.-S. Jiang, X. Tong, S. Hasegawa, S. Ino, Surf. Sci. 376 (1997) 69.
[21] X. Tong, C.-S. Jiang, K. Horikoshi, S. Hasegawa, Surf. Sci. 449 (2000) 125.
[22] S. Hasegawa, X. Tong, C.-S. Jiang, Y. Nakajima, T. Nagao, Surf. Sci. 386 (1997) 322.
[23] S. Hasegawa, S. Ino, Phys. Rev. Lett. 68 (1992) 1192.
[24] S. Hasegawa, S. Ino, Int. J. Mod. Phys. B 7 (1993) 3817.
[25] S. Hasegawa, X. Tong, S. Takeda, N. Sato, T. Nagao, Prog. Surf. Sci. 60 (1999) 89.
[26] K. Toriyama, Master Thesis, University of Tokyo, 1997 (in Japanese), unpublished.
[27] Y.L. Gavriljuk, V.G. Lifshits, O.V. Bekhtereva, S.G. Azatyan, N. Enebish, Surf. Sci. 373 (1997) 173.
[28] K. Tsuchie, T. Nagao, S. Hasegawa, Phys. Rev. B 60 (1999) 11131.
[29] M.S. Dresselhaus, G. Dresslhaus, P.C. Eklund, Science of Fullerenes and Carbon Nanotubes, Academic Press, San Diego, 1995.
[30] P. Moriarty, M.D. Upward, A.W. Dunn, Y.-R. Ma, P.H. Beton, Phys. Rev. B 57 (1998) 362.
[31] T. Nakayama, J. Onoe, K. Takeuchi, M. Aono, Phys. Rev. B 59 (1999) 12627.
[32] G. Le Lay, M. Gothelid, V.Y. Aristov, A. Cricenti, M.C. Hakansson, C. Giammichele, P. Perfetti, J. Avila, M.C. Asensio, Surf. Sci. 377–379 (1997) 1061.
[33] T. Nakayama, Doctor Thesis, University of Tokyo, 1999 (in Japanese), unpublished.
[34] K. Iizumi, K. Ueno, K. Saiki, A. Koma, in: Proc. 54th Annual Meeting of The Physical Society of Japan (Hiroshima, March) No. 2. 1999, p. 338, (in Japanese).